

# Exploring the use of Transition Path Theory in building an oil spill prediction scheme

M.J. Olascoaga<sup>1,\*</sup> and F.J. Beron-Vera<sup>2</sup>

<sup>1</sup>Department of Ocean Sciences, Rosenstiel School of Marine, Atmospheric, and Earth Science, University of Miami, FL, USA

<sup>2</sup>Department of Atmospheric Sciences, Rosenstiel School of Marine, Atmospheric, and Earth Science, University of Miami, FL, USA

Correspondence\*:  
Corresponding Author  
jolascoaga@miami.edu

## ABSTRACT

The Transition Path Theory (TPT) of complex systems has proven a robust means for statistically characterizing the ensemble of trajectories that connect any two preset flow regions, say  $\mathcal{A}$  and  $\mathcal{B}$ , directly. More specifically, transition paths are such that they start in  $\mathcal{A}$  and then go to  $\mathcal{B}$  without detouring back to  $\mathcal{A}$  or  $\mathcal{B}$ . This way, they make an effective contribution to the transport from  $\mathcal{A}$  to  $\mathcal{B}$ . Here, we explore its use for building a scheme that enables predicting the evolution of an oil spill in the ocean. This involves appropriately adapting TPT such that it includes a reservoir that pumps oil into a typically open domain. Additionally, we lift up the restriction of the oil not to return to the spill site en route to a region that there is interest to be protected. TPT is applied on oil trajectories available up to the present, e.g., as integrated using velocities produced by a data assimilative system or as inferred from high-frequency radars, to make a prediction of transition oil paths beyond, without relying on forecasted oil trajectories. As a proof of concept we consider a hypothetical oil spill in the Trion oil field, under development within the Perdido Foldbelt in the northwestern Gulf of Mexico, and the *Deepwater Horizon* oil spill. This is done using trajectories integrated from climatological and hindcast surface velocity and winds as well as produced by satellite-tracked surface drifting buoys, in each case discretized into a Markov chain that provides a framework for the TPT-based prediction.

**Keywords:** oil spill, Transition Path Theory, Markov chain

## 1 INTRODUCTION

The *Transition Path Theory* [1, 2] provides a rigorous statistical means for highlighting the dominant pathways connecting two metastable states of a complex dynamical system. That is, instead of studying the individual complicated paths connecting them, TPT concerns their average behavior and shows their dominant transition channels. TPT produces a much cleaner picture, and hence much easier to interpret, allowing one to frame the relative contribution of myriad competing paths in the presence of stochasticity.

Applications of TPT have now grown beyond the study of molecular systems [3, 4, 5, 6, 7, 8], for which it was originally conceived. Such applications involve reactions, which, to develop fully, must overcome barriers in the energy landscape. Indeed, TPT has been recently used to investigate tipping atmospheric phenomena such as sudden stratospheric warmings [9, 10]. But departing from the rare event

framing setting is possible and motivated by the fact that in other type of applications, particularly fluid mechanics, there is a basic interest of understanding how two regions (of the flow domain) are most effectively connected. With this idea in mind, TPT has been used in oceanography to bring additional insight to pollution [11] and macroalgae pathways in the ocean [12], as well as paths of the upper [13] and lower [14, 15] limbs of the meridional overturning circulation in the Atlantic Ocean.

In this paper, we explore the use of TPT in building an oil spill prediction scheme that relies on oil parcel trajectory information up to the time of the prediction. That is, the scheme assumes that time-resolved validated model velocities are available up to the present time when the prediction is made. No assumption is made on the availability of forecasted velocities from numerical models. The basic assumption is that environmental conditions, namely, near-surface ocean currents and winds, prior to the prediction instant prevail for some time past this instant. The scheme, however, enables updating the predictions over time as new velocity information becomes available. This idea was put forth in [16] to predict sudden changes in the shape of the oil slick from the *Deepwater Horizon* spill, yet using an approach different than the that one proposed here based on TPT. The framework for TPT is a Markov chain on boxes resulting by discretizing of the oil parcel motion. Such a framework has been used in [17], but to describe general oil spill scenarios based on climatological velocities.

The rest of the paper is organized as follows. In Section 2.1 we review the formulae of TPT for autonomous, i.e., time-homogeneous, discrete-time Markov chains. Section 2.2 presents an extension of the standard TPT setup for the case of oil spills. The TPT-based prediction scheme is presented in Section 2.3. In Section 3 we test the scheme assuming a hypothetical spill in the northwestern Gulf of Mexico (Section 3.1) and by considering the *Deepwater Horizon* oil spill (Section 3.2). Finally, in Section 4 we present a summary of the paper along with several ideas as to how improving the proposed prediction scheme.

## 2 METHODS

### 2.1 Transition Path Theory for Markov chains

Let  $X_n$  denote the position of a random walker at discrete time  $nT$ ,  $n \in \mathbb{Z}$ ,  $T > 0$ , in a *closed* two-dimensional domain  $\mathcal{D}$  covered by  $N$  disjoint boxes  $\{B_1, \dots, B_N\}$ . (For simplicity, we will avoid using a different notation for the covering of  $\mathcal{D}$ . Also,  $X_n \in B_i$  and  $i : B_i \in \mathcal{D}$  (or similar) will be simplified to  $X_n = i$  and  $i \in \mathcal{D}$ , respectively.) Then  $\Pr(X_{n+1} = j) = \sum_{i \in \mathcal{D}} P_{ij} \Pr(X_n = i)$  where

$$P_{ij} := \Pr(X_{n+1} = j \mid X_n = i), \quad \sum_{j \in \mathcal{D}} P_{ij} = 1 \forall i \in \mathcal{D}, \quad (1)$$

which describes the proportion of probability mass in  $B_i$  that flows to  $B_j$  during  $T$ , called a *transition time step*. The row-stochastic matrix  $P = (P_{ij})_{i,j \in \mathcal{D}}$  is called the *transition matrix* of the (two-sided) autonomous, discrete-time Markov chain  $\{X_n\}_{n \in \mathbb{Z}}$ . We assume that the process is ergodic and mixing with respect to the *stationary distribution*  $\pi = (\pi_i)_{i \in \mathcal{D}}$ . Namely, a componentwise positive vector on  $\mathcal{D}$ , seen as an  $N$ -dimensional state (vector) space, which is invariant and limiting. Normalized to a probability vector, i.e., such that  $\sum_{i \in \mathcal{D}} \pi_i = 1$ ,  $\pi$  satisfies  $\pi = \pi P = \mathbf{v} P^\infty$  for any probability vector  $\mathbf{v}$  (on  $\mathcal{D}$ ). For details, cf. [18].

The *Transition Path Theory* (TPT) provides a rigorous characterization of the ensemble of trajectory pieces, which, flowing out last from a region  $\mathcal{A} \subset \mathcal{D}$ , next go to a region  $\mathcal{B} \subset \mathcal{D}$ , disconnected from  $\mathcal{A}$ . Such trajectory pieces are called *reactive trajectories*. This terminology [1, 2] originates in chemistry,

where  $\mathcal{A}$  (resp.,  $\mathcal{B}$ ) is identified with the reactant (resp., product) of a chemical transformation. The fluidic interpretation of reactive trajectories is of trajectories of *diffusive tracers* that contribute to the bulk transport between  $\mathcal{A}$  and  $\mathcal{B}$ , which can be thought as a *source* and a *sink* or *target*, respectively.

**REMARK 1.** For a diffusive tracer to fit the above interpretation, its evolution must be described by a stationary stochastic process, i.e., an advection–diffusion equation with a steady velocity. This can be seen by discretizing its Lagrangian motion using, for instance, Ulam’s method (e.g., [19, 20]), which consists in projecting the probability density of finding tracer on a given spatial location at a discrete time instant onto a finite-dimensional vector space spanned by indicator functions on boxes, which, covering the flow domain, are normalized by their Lebesgue measure (area) [21]. The boxes represent the states of the autonomous, discrete-time Markov chain that the diffusive tracer parcels wander about.

The main objects of TPT are the *forward*,  $\mathbf{q}^+ = (q_i^+)_{i \in \mathcal{D}}$ , and *backward*,  $\mathbf{q}^- = (q_i^-)_{i \in \mathcal{D}}$ , *committor probabilities*. These give the probability of a trajectory initially in  $B_i$  to first enter  $\mathcal{B}$  and last exit  $\mathcal{A}$ , respectively. Namely,

$$q_i^\pm := \Pr(t_{\mathcal{B}}^\pm < t_{\mathcal{A}}^\pm \mid X_0 = i) \quad (2)$$

where

$$t_{\mathcal{S}}^\pm := \pm \inf\{nT \geq 0 : X_n^\pm \in \mathcal{S}\}, \quad \inf \emptyset := \infty, \quad (3)$$

with the plus (resp., minus) sign denoting (random) *first entrance* (resp., *last exit*) time of a set  $\mathcal{S} \subset \mathcal{D}$ . Here,  $\{X_n^-\}_{n \in \mathbb{Z}}$  is the original chain,  $\{X_n\}_{n \in \mathbb{Z}} = \{X_n^+\}_{n \in \mathbb{Z}}$ , but traversed in backward time, i.e.,  $X_n^- := X_{-n}$ . The reversed chain’s transition matrix,  $P^- = (P_{ij}^-)_{i,j \in \mathcal{D}}$ , where

$$P_{ij}^- := \Pr(X_{n+1}^- = j \mid X_n^- = i) = \Pr(X_n = j \mid X_{n+1} = i) = \frac{\pi_j}{\pi_i} P_{ji}, \quad (4)$$

since  $\Pr(X_n = i) = \pi_i$ . The committors are fully determined by  $P$  and  $\pi$  by solving two linear algebraic systems with appropriate boundary conditions [4, 22], concisely written as:

$$q_i^\pm = \sum_{j \in \mathcal{D}} P_{ij}^\pm q_j^\pm, \quad i \in \mathcal{D} \setminus \mathcal{A} \cup \mathcal{B}, \quad q_{i \in \mathcal{A}}^\pm = \delta_{1 \mp 1, 2}, \quad q_{i \in \mathcal{B}}^\pm = \delta_{1 \pm 1, 2}, \quad (5)$$

where  $P_{ij}^+ = P_{ij}$  and  $\delta_{kl}$  is Kronecker’s delta.

Four main statistics of the ensemble of reactive trajectories are expressed using the committor probabilities as follows:

1. The *reactive probability distribution*,  $\pi^{AB} = (\pi_i^{AB})_{i \in \mathcal{D}}$ , where  $\pi_i^{AB}$  is defined as the joint probability that a trajectory is in box  $B_i$  while transitioning from  $\mathcal{A}$  to  $\mathcal{B}$ . This is computed as [4, 22]

$$\pi_i^{AB} = q_i^- \pi_i q_i^+. \quad (6)$$

2. The *reactive probability flux*,  $f^+ = (f_{ij}^+)_{i,j \in \mathcal{D}}$ , where  $f_{ij}^+$  gives the *net* flux of trajectories going through  $B_i$  and  $B_j$  in one time step on their direct way from  $\mathcal{A}$  to  $\mathcal{B}$ , indicates the dominant transition channels from  $\mathcal{A}$  to  $\mathcal{B}$ . According to [3, 22], this is computed as:

$$f_{ij}^+ := \max \left\{ f_{ij}^{AB} - f_{ji}^{AB}, 0 \right\}, \quad f_{ij}^{AB} = q_i^- \pi_i P_{ij} q_j^+. \quad (7)$$

3. The *reactive rate* of trajectories leaving  $\mathcal{A}$  or entering  $\mathcal{B}$ , defined as the probability per time step of a reactive trajectory to leave  $\mathcal{A}$  or enter  $\mathcal{B}$ , is computed as [4, 22]

$$k^{AB} := \sum_{i \in \mathcal{A}, j \in \mathcal{D}} f_{ij}^{AB} \equiv \sum_{i \in \mathcal{D}, j \in \mathcal{B}} f_{ij}^{AB}. \quad (8)$$

Divided by the transition time step  $T$ ,  $k^{AB}$  is interpreted as the *frequency* of transition paths leaving  $\mathcal{A}$  or entering  $\mathcal{B}$  [11].

4. Finally, the *reaction duration*,  $t^{AB}$ , of a transition from  $\mathcal{A}$  to  $\mathcal{B}$  is obtained by dividing the probability of being reactive by the reactive rate, interpreted as a frequency [22]:

$$t^{AB} := \frac{\sum_{i \in \mathcal{D}} \pi_i^{AB}}{k^{AB}/T}. \quad (9)$$

## 2.2 Adapting Transition Path Theory to the oil spill problem

Let  $x(t)$  represent a very long *oil* parcel trajectory visiting every box of the covering of  $\mathcal{D}$ . Assume that this not different than any other trajectory, namely, it represents a realization of a stationary random process. Then  $x(t)$  and  $x(t + T)$  at any  $t > 0$  provide observations for  $X_n$  and  $X_{n+1}$ , respectively. Under these conditions, we can approximate  $P_{ij}$  via counting transitions between covering boxes, viz.,

$$P_{ij} \approx \frac{\#\{x(t) \in B_i, x(t + T) \in B_j\}}{\#\{x(t) \in B_i, \}}, t : \text{any}. \quad (10)$$

In general the domain  $\mathcal{D}$  potentially affected by an oil spill will represent some portion of the ocean. This makes  $\mathcal{D}$  an *open* flow domain. In such a case,  $P$  cannot be row-stochastic, which requires an adaptation of TPT. To achieve the required adaptation, we first replace  $P$  by a row-stochastic transition matrix  $\tilde{P}$  defined by

$$\tilde{P} := \begin{pmatrix} P & \mathbf{p}^{\mathcal{D} \rightarrow \omega} & \mathbf{0} \\ \mathbf{p}^{\mathcal{D} \leftarrow \omega} & 0 & 0 \\ \mathbf{p}^{\mathcal{O} \leftarrow \mathcal{R}} & 0 & p^{\mathcal{R} \rightarrow \mathcal{R}} \end{pmatrix} \quad (11)$$

on the extended  $(N + 2)$ -dimensional state space

$$\tilde{\mathcal{D}} := \mathcal{D} \cup \omega \cup \mathcal{R} \quad (12)$$

Here,  $\omega$  denotes a virtual state, called a *two-way nirvana state*, which absorbs probability mass imbalance from  $\mathcal{D}$  and sends it back to the chain. More precisely, in (11),

$$\mathbf{p}^{\mathcal{D} \rightarrow \omega} = \left(1 - \sum_{j \in \mathcal{D}} P_{ij}\right)_{i \in \mathcal{D}} \quad (13)$$

gives the outflow from  $\mathcal{D}$ , while  $\mathbf{p}^{\mathcal{D} \leftarrow \omega}$  gives the inflow, which can be constructed, as we do below, using reentry information available from trajectory data outside  $\mathcal{D}$ . In turn,  $\mathcal{R}$  is another virtual state, called an *oil reservoir state*, from which the chain drains probability mass through the oil spill site  $\mathcal{O} \subset \mathcal{D}$ . That is,

$$\mathbf{p}^{\mathcal{O} \leftarrow \mathcal{R}} = \frac{\mathbf{1}_{\mathcal{O}}}{|\mathcal{O}|} (1 - p^{\mathcal{R} \rightarrow \mathcal{R}}), \quad (14)$$

so that  $\sum_{i \in \mathcal{D}} p_i^{\mathcal{O} \leftarrow \mathcal{R}} + p^{\mathcal{R} \rightarrow \mathcal{R}} = 1$ . (The notation  $\mathbf{1}_S$  is used to mean a vector on (the  $N$ -dimensional space given by the covering of)  $\mathcal{D}$  with ones in the entries corresponding to (subcovering)  $S \subset \mathcal{D}$  and zeros elsewhere.) Below we will expand on how to set  $p^{\mathcal{R} \rightarrow \mathcal{R}}$ . As in the standard TPT setup presented in Section 2.1, the stochastic process described by  $\tilde{P}$  in (11) is assumed to be in stationarity. The stationary distribution on  $\tilde{\mathcal{D}}$  is denoted  $\tilde{\pi}$ . (Herein a tilde is used to emphasize that the quantity in question is computed using the extended Markov chain on  $\tilde{\mathcal{D}}$ .) A caveat to note is that the Markov process on  $\tilde{\mathcal{D}}$  cannot be strictly ergodic because  $\mathcal{R}$  is never visited by a trajectory unless it starts there. Yet, this does not rule out the existence of a well-defined  $\tilde{\pi}$  (unless  $p^{\mathcal{R} \rightarrow \mathcal{R}} = 0$ , in which case  $\tilde{\pi}|_{\mathcal{R}} = 0$ , and hence  $\tilde{\pi}$  will not be strictly componentwise positive).

Now, arguably, it is the oil that reaches the coastline or any region one may want to protect what really matters, irrespective that oil trajectories visit the spill site many times in between. Call this region  $\mathcal{P} \subset \mathcal{D}$ . The former cannot be achieved by simply setting  $\mathcal{A} = \mathcal{O}$  and  $\mathcal{B} = \mathcal{P}$ .

**PROPOSITION 1.** *To achieve the desired effect, which slightly deviates us from the standard TPT setting, one must set  $\mathcal{A} = \mathcal{R} \cup \omega$  and  $\mathcal{B} = \mathcal{P}$  for the computation of  $\tilde{\mathbf{q}}^+$  for extended chain on  $\tilde{\mathcal{D}}$ , while  $\mathcal{A} = \mathcal{R}$  and  $\mathcal{B} = \mathcal{P} \cup \omega$  for the computation of  $\tilde{\mathbf{q}}^-$  (on  $\tilde{\mathcal{D}}$ ).*

Indeed, placing the source in  $\mathcal{R}$  enables oil paths visiting  $\mathcal{O}$ , and including  $\omega$  as indicated prevents trajectories from escaping the flow domain, thereby highlighting the portion that flows into  $\mathcal{P}$  through  $\mathcal{D}$  (Fig. 1). The TPT formulae in Section 2.1 remains the same with the above choices of  $\mathcal{A} \subset \tilde{\mathcal{D}}$  and  $\mathcal{B} \subset \tilde{\mathcal{D}}$ , and, of course, the use of  $\tilde{P}$  and  $\tilde{\pi}$  in place of  $P$  and  $\pi$ , respectively, in them.

Inclusion of a two-way-nirvana state is not new, as it was first applied by [11] to treat transition paths of marine debris into the subtropical oceans great garbage patches. Additional TPT applications involving this type of closure include [14, 12, 15, 13]. The use of an oil reservoir state is novel in TPT.

## 2.3 A proposal for using Transition Path Theory to predict oil paths and arrival

We propose to apply TPT such that it makes use of available oil trajectories up to the present, to make a prediction beyond, so it does not rely on forecasted oil trajectories. This follows precedent work [16], which was able to predict sudden changes in the shape of the oil slick during the *Deepwater Horizon* spill. The expectation is that such a type of prediction should be superior than that based on forecasted velocities, which are not validated by data as is the case of hindcast velocities from an analysis system. Moreover, when available, the scheme enables the use of velocities inferred from high-frequency radar measurements and even trajectories of appropriate satellite-tracked surface drifting buoys.

The proposed prediction scheme more specifically consists in applying TPT using trajectories over a few time steps prior to the prediction time, say  $t_0 = n_0 T$ . That is, we propose to compute the closed transition matrix  $\tilde{P}$  for the augmented Markov chain on  $\tilde{\mathcal{D}}$ , as given by (11), and the various TPT statistics from it according to Proposition 1, by making use of *all trajectories available over*  $t \in \{(n_0 - m)T, \dots, (n_0 - 1)T, n_0 T\}$  for some  $m \leq n_0$ . This way a prediction for the spilled oil distribution on  $t = (n_0 + 1)T$ , in direct transition into the region to be protected,  $\mathcal{P}$ , is obtained. The skeleton thereof will be provided by the two-dimensional vector field taking values at discrete positions  $x_i$ , where  $x_i$  is the center of box  $B_i \in \mathcal{D}$ , given by

$$J(x_i) := \sum_{j \in \mathcal{D}} \tilde{f}_{ij}^+ e(i, j), \quad (15)$$

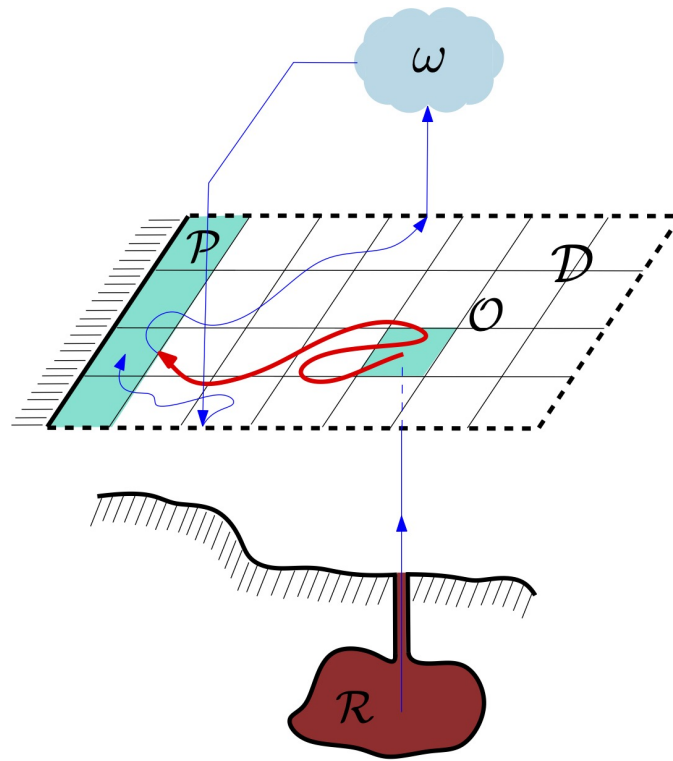


**Figure 1.** The framework for the TPT-based prediction scheme is an autonomous, discrete-time Markov chain on a state space given by the box covering of a two-dimensional, open ocean domain,  $\mathcal{D}$ , augmented by two virtual boxes or states. One state, called a two-way nirvana state and denoted by  $\omega$ , compensates for probability mass imbalances due to the openness of  $\mathcal{D}$ . The other state, called an oil reservoir state and denoted by  $\mathcal{R}$ , injects probability mass into the chain through the spill site,  $\mathcal{O} \subset \mathcal{D}$ . Highlighted in red is the restriction to  $\mathcal{D}$  of a reactive trajectory connecting  $\mathcal{R}$  with  $\mathcal{P} \subset \mathcal{D}$ , a region that there is interest in being protected, chosen to be the shoreline in the cartoon. Such a trajectory flows last from  $\mathcal{R}$  and next goes to  $\mathcal{P}$ , while being constrained to stay in  $\mathcal{D}$ , once it enters  $\mathcal{D}$ . So defined, a reactive trajectory of oil may return back many times to the spill site before reaching the protected area. TPT provides a statistical characterization of the ensemble of reactive trajectories, highlighting the dominant paths of oil into  $\mathcal{P}$ .

where  $e(i, j)$  is the (two-dimensional) unit vector pointing from  $x_i$  to  $x_j$ , the center of box  $B_j \in \mathcal{D}$ . The above is a visualization means of reactive probability flux, proposed in [22]. We will refer to (15) as the *reactive current* at position  $x_i$ . The prediction can be updated, as we will do in the examples we provide below, by computing TPT using trajectories within time windows *sliding* over the prediction time  $t_0$  (or  $n_0$ ).

In the present exploratory work, the oil evolution in every case will be obtained by pushing forward a probability vector on  $\tilde{\mathcal{D}}$  with support in  $\mathcal{R}$  at time  $t = 0$ , namely,

$$\tilde{\mathbf{o}}(0) = \frac{\tilde{\mathbf{1}}_{\mathcal{R}}}{|\mathcal{R}|}, \quad (16)$$

under right multiplication by a *nonautonomous* version of the augmented chain transition matrix  $\tilde{P}$  in (11). Denoted by  $\tilde{P}(n)$  to make explicit its dependence on  $t = nT$ , this will be constructed by *accounting for the start time  $t$  in the estimation of  $P$  in (10)*. To add a bit of extra realism, we will set  $p^{\mathcal{R} \rightarrow \mathcal{R}}$  in (11) to

$$p^{\mathcal{R} \rightarrow \mathcal{R}}(n) = \frac{1}{N - n + 1}, \quad (17)$$

representing an oil reservoir that is drying over the time interval  $t \in \{0, T, 2T, \dots, NT\}$ . Indeed, when  $n = N$ ,  $p^{\mathcal{R} \rightarrow \mathcal{R}} = 1$ , meaning that the probability mass flux into the ocean domain  $\mathcal{D}$  through the oil spill site  $\mathcal{O}$  is nil. That is, the reservoir  $\mathcal{R}$  has completely dried out by  $t = NT$ . This assumption may be adapted based on any information available about how quickly the oil reservoir may be expected to empty or a spilling oil well may be capped. The *total accumulated* oil, which flows out from  $\mathcal{R}$  into  $\mathcal{D}$  through  $\mathcal{O}$  in an uninterruptedly but decaying in time manner, at discrete time  $t = nT$  will be given by  $\mathbf{o}(n) = \tilde{\mathbf{o}}(n)|_{\mathcal{D}}$ , where

$$\tilde{\mathbf{o}}(n) = \tilde{\mathbf{o}}(0) \left( \text{Id} + \sum_{k=0}^{n-1} \prod_{l=k}^{n-1} \tilde{P}(l) \right). \quad (18)$$

Note that  $\tilde{\mathbf{o}}(n)$ , and hence  $\mathbf{o}(n)$ , does not need to be a probability vector, and the units in which  $\mathbf{o}(n)$  is measured are determined by the units assigned to  $\tilde{\mathbf{o}}(0)$ .

To incorporate the effects of a drying oil reservoir in the TPT prediction step, the autonomous  $\tilde{P}$  used in that step will have to set  $p^{\mathcal{R} \rightarrow \mathcal{R}}$  in (11) to the average value of over the corresponding time interval.

The idea of using trajectory information up to the present prevents us from using the extension of TPT for time-inhomogeneous Markov chains proposed in [22], as it might be thought to be more suitable for a prediction scheme in a naturally time-varying environment. The reason is that, as formulated, nonautonomous TPT requires unavailable trajectory information and knowledge of when  $\mathcal{P}$  will be hit by transition paths.

A final comment is reserved to the oil trajectories themselves. If  $u(x, t)$  denotes the surface ocean velocity, as output from an ocean circulation model, and  $u_{10}(x, t)$  is the wind velocity at 10-m above the sea surface, as produced by some atmospheric circulation model, the oil trajectories will here be obtained by integrating

$$\dot{x} = u(x, t) + \alpha u_{10}(x, t), \quad 0 < \alpha \ll 1, \quad (19)$$

for many initial conditions over a domain including the ocean domain  $\mathcal{D}$  of interest, so reentry information, namely, that required to evaluate  $\mathbf{p}^{\mathcal{O} \leftarrow \omega}$  in (11), is available. Equation (19) is a *minimal* law for oil parcel motion [23, 24]. It exclusively accounts for the wind action on oil parcels, neglecting the various physical and biogeochemical changes oil undergo as it spends time in the environment, collectively known as “weathering” effects [25]. Typically employed values of  $\alpha$  range from 2 to 4% [26].

## 3 RESULTS

### 3.1 Hypothetical oil spill in the Trion field

We begin by applying our proposed TPT-based prediction scheme to a hypothetical oil spill in the Trion field, located within the Perdido Foldbelt, a geological formation in the northeastern Gulf of Mexico with an important oil reservoir for ultradeepwater drilling under development [27]. This will be done by considering two different velocity representations.

In the first representation,  $u$  in (19) is chosen to be given by a daily climatology of surface velocity constructed from velocities over 18-yr (1995–2012) produced by a free-running regional configuration for the Gulf of Mexico at  $1/36^\circ$ -horizontal resolution [28] of the ocean component of the Nucleus for European Modelling of the Ocean (NEMO) system [29]. This dataset was used in [30] to investigate persistent passive tracer transport patterns using so-called climatological Lagrangian Coherent Structures (cLCSs) [31]. A main finding was the presence of a mesoscale hook-like cLCs providing a barrier for

cross-shelf transport nearly year round. Consistent with the motion of historical satellite-tracked drifting buoys, with the majority of them including a drogue, albeit shallow (cf. Miron et al. [32] for details), synthetic drifters originating beyond the shelf were found to be initially attracted to this cLCS as they spread anticyclonically and eventually over the deep ocean. In [30] it is noted that this should have implications for the mitigation of contaminant accidents such as oil spills. This picture, however, may be altered for oil, as this is expected to be influenced by the wind action, which in [30] was not accounted for, when winds are strong. To evaluate their effect we need a representation for  $u_{10}$  in (19), which is chosen to be provided by daily climatological wind velocity at 10-m height from the European Centre for Medium-Range Weather Forecasts (ECMWF) atmospheric reanalysis ERA-Interim [33].

In Fig. 2 we present our first set of results. These are based on the use of trajectories obtained by numerically integrating (19), with the daily climatological NEMO+ECMW velocity data above, using a 4th-order Runge–Kutta scheme with cubic interpolation in space and time. The integrations, reinitialized every day along the month of February, span  $T = 1$  d. We consider initial conditions distributed uniformly over an ocean domain larger (by  $1^\circ$  to the east and south) than that one ( $\mathcal{D}$ ) contained inside  $[98^\circ\text{W}, 93^\circ\text{W}] \times [24^\circ\text{S}, 30^\circ\text{N}]$ , shown in Fig. 2. To evaluate the transition matrix on  $\mathcal{D}$ , using (10), we cover  $\mathcal{D}$  with boxes of about  $1/6^\circ$ -side, including roughly 100 test points per box when trajectories initialized once are only considered. The transition time step  $T = 1$  d guarantees sufficient loss of memory into the past for the Markovian assumption to hold; indeed, the typical decorrelation timescale on ocean surface is not longer than 1 d as estimated from drogued drifting buoys [34], and is likely to be even shorter when the wind action is accounted for. Stationary of the Markov chain on the extended domain  $\tilde{\mathcal{D}}$  is checked numerically. That is, we check that the largest eigenvalue of the transition matrix  $\tilde{P}$  has multiplicity 1, and is equal to 1, to numerical precision. However, in the computation of  $\mathcal{P}$ , namely, the transition matrix on the open domain  $\mathcal{D}$ , we make sure to allow as much communication as possible along the corresponding Markov chain by applying Tarjan's [35] algorithm on the associated directed graph, as we have done earlier work (e.g., [32, 36, 21, 37]). This can result in some boxes of the covering of the ocean domain to be excluded, particularly when dealing with observed (satellite-tracked) trajectories, as we consider in Section 3.2, below.

With  $\mathcal{O}$ , the oil spill site, taken to be a box of the covering of  $\mathcal{D}$  closest to the Trion field and  $\mathcal{P}$ , the region to be protected, taken to be the coastal boxes, the top row of Fig. 2 shows the *predicted* reactive rate of (oil) trajectories entering each box of  $\mathcal{P}$  for selected times since since 1 February when the oil spill is hypothetically initiated. Specifically, we show this normalized to a probability vector on  $\mathcal{D}$ , viz.,

$$\mathbf{k} := \sum_{i \in \mathcal{P}} \frac{\tilde{k}^{\mathcal{R}B_i}}{\sum_{i \in \mathcal{P}} \tilde{k}^{\mathcal{R}B_i}} \mathbf{1}_{B_i} \Big|_{\mathcal{P}}, \quad \tilde{k}^{\mathcal{R}B_i} = \sum_{l \in \tilde{\mathcal{D}}} \tilde{f}_{li} = \sum_{l \in \tilde{\mathcal{D}}} \tilde{f}_{il}, \quad i \in \mathcal{P}, \quad (20)$$

where the TPT computation follows Proposition 1. More precisely, in the TPT calculation we apply Proposition 1 for each  $i \in \mathcal{P}$ , i.e., with  $\mathcal{P}$  replaced by  $i \in \mathcal{P}$ . The transition matrix of the augmented chain in  $\tilde{\mathcal{D}}$ , given by (11), is computed using trajectories over  $t \in \{t_0 - 2T, t_0 - T, t_0\}$  for every  $t_0$  in Fig. 2. The coastal boxes that are predicted to be most affected by the oil spill correspond are those where components of  $\mathbf{k}$  in (20) take the largest values. Note, in this case, that the predicted coastal boxes to be most affected change over time, moving from the boxes corresponding to the Mexican state of Tamaulipas north, toward the international border with the United States. This is consistent with the updated reactive current predictions and, most importantly, with the portion of the simulated spilled oil distribution directed into the coastline. This is depicted in the bottom row of Fig. 2. More specifically, the heatmap in each panel



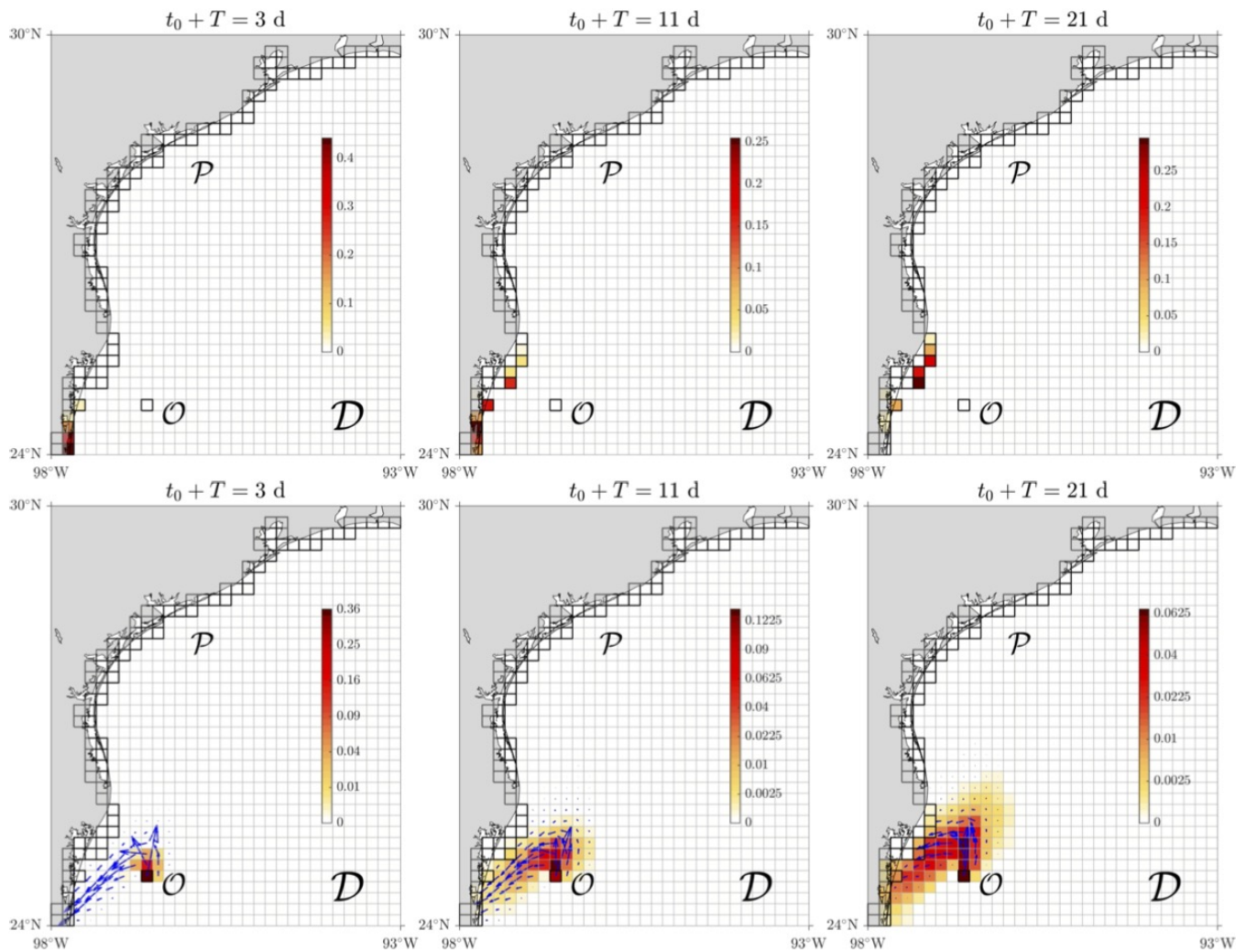


**Figure 2.** (top panels) Based on the daily climatological NEMO+ECMW oil velocity model, predictions on time  $t = t_0$  of (normalized) reactive rates of arrival of transition paths, through the open northwestern Gulf of Mexico domain  $\mathcal{D}$  and into the coastline ( $\mathcal{P}$ ), of oil emerging from a hypothetical open well in the Trion field ( $\mathcal{O}$ ), located within the Perdido Foldbelt, on  $t = 0$ , corresponding to February 1. The transition time step,  $T = 1$  d. (bottom panels) Relative distribution of accumulated oil on  $t = t_0 + T$ , overlaid with predicted (on  $t = t_0$ ) reactive currents, indicating transition oil paths into  $\mathcal{P}$ .

is of  $\mathbf{o}(n_0 + 1) = \tilde{\mathbf{o}}(n_0 + 1)|_{\mathcal{D}}$ , with  $\tilde{\mathbf{o}}(n)$  given in (18), but normalized to a probability vector, giving the *relative distribution* of oil that has accumulated on  $\mathcal{D}$  at time  $t = t_0 + T = (n_0 + 1)T$ . Overlaid on each heatmap are the predicted reactive currents (15) on each  $t_0$ . These are seen to anticipate,  $T = 1$ -d in advance, the motion of the oil directed into the coastline quite well.

An important observation is that the main responsible for this motion is the wind action on the oil, which makes it to bypass the cross-shelf transport barrier for passive tracers shown [30] to be supported nearly year-round by the climatological NEMO surface ocean velocity field. Indeed, the winter season is dominated by “nortes” [38]. These are strong, predominantly northerly winds suddenly produced after the passage of a cold fronts, which, imprinted in the daily climatology, promote the accumulation of the oil toward the coastline.

In addition to predicting the transition paths of oil the into the coastline, TPT can give a prediction for the arrival time of the oil. Using the reaction duration formula (9), but on the extended Markov chain on  $\tilde{\mathcal{D}}$

and for each  $i \in \mathcal{P}$ , as done to compute the reaction rate (20), we compute on  $t_0 = 2$  d, the first time a prediction can be made, that

$$\min_{i \in \mathcal{P}} \{\tilde{t}^{\mathcal{R}B_i}\} = \min_{i \in \mathcal{P}} \left\{ \frac{\sum_{l \in \tilde{\mathcal{D}}} \tilde{\pi}_l^{\mathcal{R}B_i}}{\tilde{k}^{\mathcal{R}B_i}/T} \right\} \approx 14 \text{ d.} \quad (21)$$

This early prediction turns out to be somewhat longer than the actual arrival time to the coast, which happens around 11-d after the (simulated) oil started. This assessment is rough, based on when oil probability mass is found for the first in a coastal box, independent of how much. With this in mind, early prediction (21) is not that off at all. But one may wonder if it could be updated with time, i.e., as newer data becomes available. This is hopeless using (9), as it computes the duration of the whole reaction from source to target, which are fixed in space. However, the desired update of the arrival time prediction may indeed be accomplished. We discuss how in the last section.

The second representation for  $u$  in (19) that we consider is provided by hourly surface ocean velocity output from the HYCOM (HYbrid-Coordinate Ocean Model) + NCODA (Navy Coupled Ocean Data Assimilation) Gulf of Mexico 1/25° Analysis (GOMu0.04/expt\_90.1m000) [39]. For  $u_{10}$  in (19) we use three-hourly wind velocity, 10-m above the sea surface, from the National Centers for Environmental Prediction (NCEP) operational Global Forecast System (GFS) analysis and forecast at 1/4°-horizontal resolution [40]. In neither case we considered forecasted velocities, but a record, from 22 July 2022 through 8 August 2022, of *hincast* velocities, i.e., as produced by the systems while they assimilated observations “on the fly” to make the forecasts. The TPT setup for the HYCOM+NCEP oil velocity is similar to that for the climatological NEMO+ECMWF oil velocity. For instance, trajectory integrations are reinitialized daily and span  $T = 1$  d, and the number of boxes of the domain partition is similar with a comparable number of test points per box. Unlike the climatological case, the time origin ( $t = 0$ ) of the oil spill simulation corresponds to a specific day of the current year, chosen to be 22 July 2022. The simulation extends out to 8 August 2022. Covering a summer time period, it is not affected by “nortes” wind events, which prevail in winter. The results are shown in Fig. 3. As can be expected, an important difference with those shown in Fig. 2 is a stronger influence of the cross-shelf transport barrier for passive tracers on the distribution of the simulated oil, which, while eventually reaching the coastline, by  $t = 16$  d it starts to develop a hook-like shape pointing into the open ocean, similar to that described in [30]. This happens after part of the oil is trapped in an anticyclonic circulation. The predicted arrival location on  $t_0 = 2$  d falls quite close to the arrival location, which takes place between the southern Texas cities of Corpus Christi and Galveston on  $t \approx 9$  d. The early prediction (on  $t_0 = 2$  d) of arrival time is  $t \approx 6$  d, which is shorter than the arrival time, calling for an update.

Overall the above results provide support to our proposed TPT-based oil spill prediction scheme, based on the assumption that the motion prior to the prediction time is representative of motion beyond it, for some time, which we test against observations in the section that follows.

### 3.2 The Deepwater Horizon oil spill

The basic assumption on which the TPT-based oil prediction scheme builds on, namely, that environmental conditions prior to the prediction time can be prolonged beyond it, for some time, is here tested using oil arrival time estimates for the *Deepwater Horizon* spill [41]. Shown in the heatmap in the center panel of Fig. 4, the arrival time estimates are inferred using available satellite images of the oil slick, as produced by the National Oceanic and Atmospheric Administration (NOAA) National Environmental Satellite Data

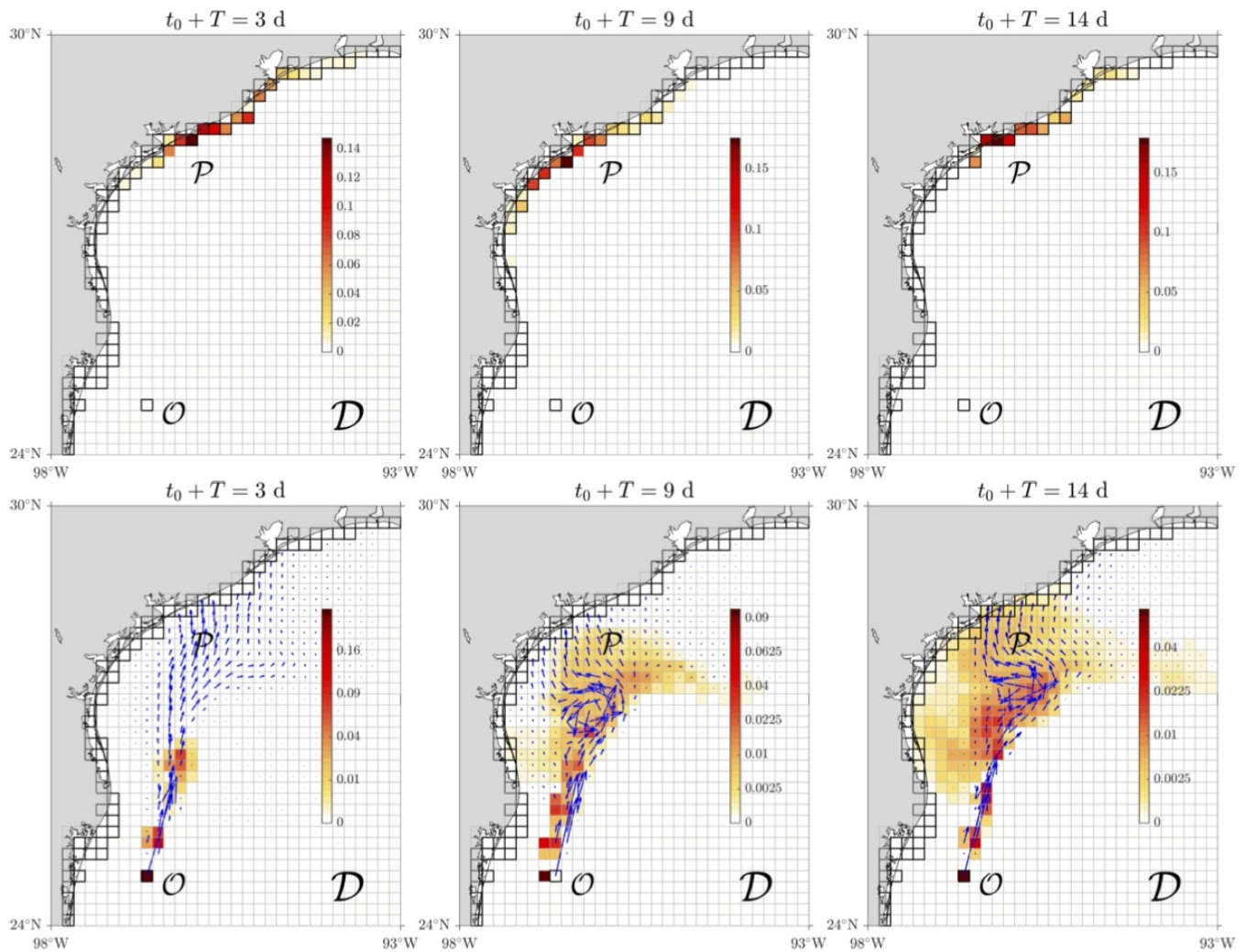


**Figure 3.** As in Fig. 2, but based on the NEMO+ECMWF oil velocity model and  $t = 0$  corresponding to 22 July 2022.

and Information Service (NESDIS) Marine Pollution Surveillance Program [42]. The time origin is 22 April 2010, when the Macondo well started to spill oil due to the sinking of the mobile offshore rig after an explosion caused by a blowout two days before [41]. The value assigned to each colored pixel corresponds to the first time (in d) the oil visited that pixel.

Four TPT-based estimates, based on four different Markov chains, of the arrival time are shown in Fig. 4, two in the top panels and two in bottom panels. More specifically, these are reaction durations (9) into each box ( $B_i$ ) of the set  $\mathcal{S}$  of the domain covering ( $\mathcal{D}$ ) that most closely intersects the region in the center panel of Fig. 4 where the oil was observed to be occupied in the satellite imagery. More specifically, we show

$$\mathbf{t} := \sum_{i \in \mathcal{S}} \tilde{t}^{R_{B_i}} \mathbf{1}_{B_i} \Big|_{\mathcal{S}}, \quad (22)$$

computed using Proposition 1 with  $\mathcal{P}$  replaced by  $i \in \mathcal{S}$ . The Markov chains are constructed as follows.

For the top panels of Fig. 4, we use  $T = 1$  d-long trajectories integrated from (19) in the interval 22 April 2010 through 29 April 2010, the day when the satellite images record reveal oil on the surface for the first

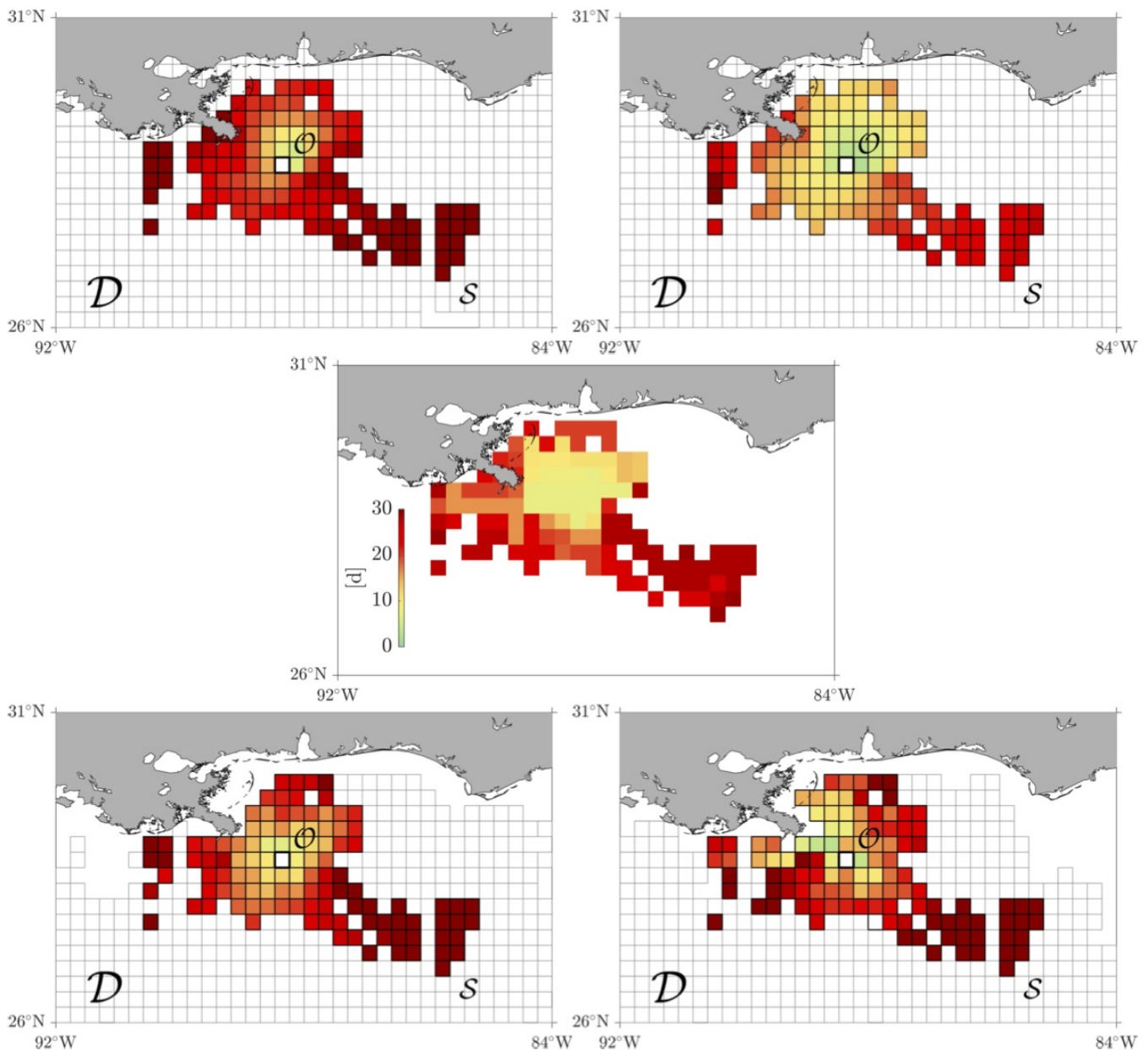


**Figure 4.** Estimated from satellite images of the *Deepwater Horizon* oil slick, time to first find oil on the surface of the ocean since the 22 April 2010, when the spill started to spill from the Macondo well (center panel), along with reaction duration of transition paths into each box of the subset  $S$  of the domain covering  $D$  that most closely intersects the region visited by the surfaced oil according to: trajectories integrated from surface NCOM velocities (top-left panel) and the latter with the addition of 3% NOAA/NCEI windage (top-right panel) over a period of 7 d prior the first time oil was found on the ocean surface on 29 April 2010; and trajectories produced by historical satellite-tracked surface drifters with drogue present (bottom-left panel) and absent (bottom-right panel).

time (since the spill started, on 22 April 2010). For both panels we use  $u$  in (19) represented by daily surface ocean velocities produced by the experimental real-time Intra-Americas Sea Nowcast/Forecast System (IASNF) at  $1/25^\circ$ -horizontal resolution, which is based on the U.S. Naval Coast Ocean Model (NCOM) [43]. In turn, the wind ( $u_{10}$ ) velocity representation is obtained from daily  $1/4^\circ$ -horizontal resolution winds at 10 m from the NOAA/National Centers for Environmental Information (NCEI) Blended Sea Winds product [44]. The difference between the top-left and right panels is that in the former the oil model velocity



uses  $\alpha = 0$ , i.e., the wind effect is shut off, and in the latter  $\alpha = 0.03$ , as we have set above. The size of each box of the covering is of  $1/25^\circ \times 1/25^\circ$ , and the number of test points per box is (roughly) 100.

For the bottom panels of Fig. 4, we consider pieces of length  $T = 1\text{d}$  of historical, i.e., available since 1992 to date, satellite-tracked trajectories of surface drifting buoys from the NOAA Global Drifter Program (GDP) [45] with the following distinction: in the left panel, we consider drifters that have their (15-m-long) drogues (sea anchors) attached at all times, while in the right panel, only those that do not have a drogue attached during the extent of the record (because this has been lost at the beginning of the record, after deployment, as assessed by the drogue presence algorithm of [46], or because the drifter was intentionally deployed undrogued). The size of each box of the covering is of  $1/25^\circ \times 1/25^\circ$  for the drogued and the undrogued drifters. The number of test points per box is small compared to that of the simulated oil trajectories, with only about 10 test points per box.

Comparison of the top-right panel of Fig. 4 with the center panel reveals that our assumption on that simulated trajectories up to the prediction time can be used to indeed make reliable predictions (beyond) holds quite well, at least for environmental conditions prevalent during the *Deepwater Horizon* spill, and during the timespan covered by the satellite imagery of the oil slick. In this case, windage in the minimal oil parcel trajectory model (19) does not dramatically impact the TPT-based computation, as can be seen from the comparison of the top-right panel with top-left panel. Recall that these use trajectories integrated over 7-d prior to first time oil is observed on the ocean surface and that the satellite oil images record extends for 30 d. Moreover, even TPT results based on historical drifter trajectories are reasonable, irrespective of whether the drifters are drogued or undrogued, as it follows from the inspection of the bottom panels of Fig. 4. These results might not come as a big surprise, as an analysis of daily climatological model velocities were successful in reproducing the “tiger tail” shape produced by the *Deepwater Horizon* oil slick [31]. Similarly, the analysis of altimetry-derived surface ocean velocities was capable of reproducing a similar shape into which drifting buoys from the Grand Lagrangian Deployment (GLAD) organized along [47].

Clearly, the above results for the *Deepwater Horizon* oil spill, the largest and best document oil spill, may not be made extensible to other oil spills in other regions of the ocean and year seasons with more variable environmental conditions reigning. Yet, they are an encouraging sign of the validity of the assumption on which our TPT-based oil prediction scheme builds on. In such more variable environments, a more sophisticated model than (19) may be needed and there is also ample space to improving the TPT setup. We highlight possible or required improvements below.

## 4 SUMMARY AND CONCLUDING REMARKS

In this paper, we have given the first steps toward building an oil spill prediction scheme based on the use of Transition Path Theory (TPT) for autonomous, discrete-time Markov chains on boxes, which cover a typically open flow domain, an result under an appropriate discretization of the oil motion, assumed to be described by a stationary stochastic process, namely, to obey an advection–diffusion with a steady velocity. Transition paths highlight the main conduits of communication between a source and a target in the phase of a dynamical system under noise, and thus they can be used to unveil the main routes of oil from an accidental spill in the ocean into a region that needs protection.

The basic premise on which the TPT-based oil prediction scheme is that trajectory information up to the prediction time can be used to infer oil motion beyond it. The TPT setup deviates from the standard TPT setup in that one needs to cope with the openness of ocean flow domain where a spill takes place, which is

accounted for by the addition of a virtual box (state) that compensates for probability mass imbalances, and also with a way to represent the injection of oil in to the open flow domain, which is done via the addition of another virtual state representing an oil reservoir. The scheme was tested by considering a hypothetical oil spill in the Trion field, located within the Perdido Foldbelt in the northwestern Gulf of Mexico, and the *Deepwater Horizon* oil spill, giving good signs of its validity.

Several improvements to the proposed scheme are possible or required. These should help increasing the quality of the predictions, particularly under environmental conditions more variable than those of the situations considered here.

- In the examples considered, the prediction time increment, say  $\Delta t_0$ , was chosen to be equal to the transition time step ( $T$ ). For the Markovianity assumption to be fulfilled,  $T$  should not be taken shorter than 1 d, the typical Lagrangian decorrelation time in the surface ocean. However, there is no restriction on the choice of  $\Delta t_0$  and the frequency of prediction updates may be higher than daily.
- In a similar manner as the prediction of transition paths of oil into the region one desires to protect are updated over time, the duration of the paths should be updated, as it is not just where oil will end that is important to know, but when it will arrive at the protected area. This will require one to compute the reaction duration into the target region from any place in between it and the source. Mathematically, this is given by the expectation of the random time to first enter the target conditioned on starting on any box (state) of the chain while the trajectory is reactive. A collection of such boxes can be chosen to be those where the updated reaction distribution (6), which tells one where the reactive flux bottlenecks, acquires the largest values. There currently is no TPT formula that accounts for this in the case of the Markov chain setting of this paper, but one can be derived by combining potential theory with a Sisyphus chain, which agrees with the original chain when this is reactive and is mapped to a nirvana state when is not [Luzie Helfmann, 2022, private communication]. For diffusion processes, a related statistic is derived in [10].
- Another aspect that we have not accounted for is oil beaching. This is an additional source of openness of the flow domain. Beaching has been incorporated in a physically consistent manner in the problem of plastic pollution [11]. Such a solution does not seem appropriate for the oil problem, and beaching may necessary result in a nonstationary Markov chain. The nonautonomous extension of TPT in [22] does not require the Markov chain to be in stationary, which may provide a resolution to this aspect. However, nonautonomous TPT requires trajectory information past the prediction time, and thus a different strategy to cope with beaching will need to be designed.
- Last but not least is the oil parcel trajectory model. We have considered the minimal possible model, which only accounts for windage in a bulk manner. The typically used 3% windage accounts for the effects wave-induced Stokes drift, which may be explicitly added to the ocean surface velocity with the corresponding reduction of the windage. The Stokes drift may be obtained from a wave model. The full ocean surface plus wave-induced drift is measured, partially at least [48, 49], by high-frequency radars, which, when available, may me be easily incorporated. Additional improvements may be provided by the Maxey–Riley theory for floating material on the ocean surface [50, 51], which includes a law for windage depending on buoyancy in closed form, or consideration of the output from an oil spill trajectory model like OpenDrift [52], which accounts for weathering effects (e.g., [17, 53]). The trajectories produced by the minimal model or improvements thereof may be combined with trajectories of satellite-tracked with appropriate drifting buoys, if these are deployed in the area where the oil spill takes place.

## AUTHOR CONTRIBUTIONS

The authors equally contributed to the paper.

## FUNDING

Support for this work was provided by Consejo Nacional de Ciencia y Tecnología (CONACyT)–Secretaría de Energía (SENER) as part of the Consorcio de Investigación del Golfo de México (CIGoM).

## ACKNOWLEDGMENTS

We thank Luzie Helfmann and Péter Koltai for discussions on adapting TPT to the oil spill problem, and Joaquin Triñanes for making available to us the *Deepwater Horizon* oil spill imagery.

## DATA AVAILABILITY STATEMENT

The ECMWF/ERA Interim wind reanalysis can be obtained from <https://apps.ecmwf.int/datasets/data/interim-full-daily/levtype=sfc/>. The Gulf of Mexico HYCOM+NCODA analysis data are available at <https://www.hycom.org/data/gomu0pt04/expt-90pt1m000>. The NCEP/GFS wind data can be retrieved from <https://www.ncei.noaa.gov/products/weather-climate-models/global-forecast>. Digitized versions of the observed surface ocean oil distribution images during the *Deepwater Horizon* spill are available at <https://satepsanone.nesdis.noaa.gov/pub/OMS/disasters/DeepwaterHorizon/composites/2010/>. The NCOM/IASNFS output is available from <https://www.northerngulfinstitute.org/edac/oceanNomads/IASNFS.php>. The NOAA/NEIC wind data are available from <https://coastwatch.pfeg.noaa.gov/erddap/griddap/ncdcOwCIm9505.html>. The NOAA/GDP drifter data are available at <https://www.aoml.noaa.gov/phod/gdp/>.

## REFERENCES

- [1] E W, Vanden-Eijnden E. Towards a theory of transition paths. *J. Stat. Phys.* **123** (2006) 503–623.
- [2] E W, Vanden-Eijnden E. Transition-path theory and path-finding algorithms for the study of rare events. *Annu. Rev. Phys. Chem.* **61** (2010) 391–420.
- [3] Noé F, Schütte C, Vanden-Eijnden E, Reich L, Weikl TR. Constructing the equilibrium ensemble of folding pathways from short off-equilibrium simulations. *Proceedings of the National Academy of Sciences* **106** (2009) 19011–19016.
- [4] Metzner P, Schütte C, Vanden-Eijnden E. Transition path theory for Markov jump processes. *Multiscale Modeling & Simulation* **7** (2009) 1192–1219.
- [5] Meng Y, Shukla D, Pande VS, Roux B. Transition path theory analysis of c-src kinase activation. *Proceedings of the National Academy of Sciences* **113** (2016) 9193–9198.
- [6] Thiede EH, Giannakis D, Dinner AR, Weare J. Galerkin approximation of dynamical quantities using trajectory data. *The Journal of Chemical Physics* **150** (2019) 244111.
- [7] Liu Y, Hickey DP, Minter SD, Dickson A, Calabrese Barton S. Markov-state transition path analysis of electrostatic channeling. *The Journal of Physical Chemistry C* **123** (2019) 15284–15292.
- [8] Strahan J, Antoszewski A, Lorpai boon C, Vani BP, Weare J, Dinner AR. Long- time-scale predictions from short-trajectory data: A benchmark analysis of the trp-cage miniprotein. *Journal of Chemical Theory and Computation* **17** (2021) 2948–2963.

- [9] Finkel J, Abbot DS, Weare J. Path properties of atmospheric transitions: Illustration with a low-order sudden stratospheric warming model. *Journal of the Atmospheric Sciences* **77** (2020) 2327–2347.
- [10] Finkel J, Webber RJ, Gerber EP, Abbot DS, Weare J. Learning forecasts of rare stratospheric transitions from short simulations. *Monthly Weather Review* **149** (2021) 3647–3669.
- [11] Miron P, Beron-Vera FJ, Helfmann L, Koltai P. Transition paths of marine debris and the stability of the garbage patches. *Chaos* **31** (2021) 033101.
- [12] [Dataset] Beron-Vera FJ, Olascoaga MJ, Putman NF, Trinanes J, Lumpkin R, Goni G. Dynamical geography and transition paths of Sargassum in the tropical Atlantic. Submitted to *Chaos*; e-preprint: <https://doi.org/10.21203/rs.3.rs-1594768/v1> (2022).
- [13] Drouin KL, Lozier MS, Beron-Vera FJ, Miron P, Olascoaga MJ. Surface pathways connecting the South and North Atlantic Oceans. *Geophysical Research Letters* **49** (2022) e2021GL096646.
- [14] Miron P, Beron-Vera FJ, Olascoaga MJ. Transition paths of North Atlantic Deep Water. *J. Atmos. Oce. Tech.* **39** (2022) 959–971.
- [15] [Dataset] Beron-Vera FJ, Olascoaga MJ, Helfmann L, Miron P. Sampling-dependent transition paths of Iceland–Scotland Overflow water. Submitted to *J. Phys. Oceanogr.*; e-preprint: <https://doi.org/10.48550/arXiv.2208.09499> (2022).
- [16] Olascoaga MJ, Haller G. Forecasting sudden changes in environmental pollution patterns. *Proc. Nat. Acad. Sci. USA* **109** (2012) 4738–4743.
- [17] Pérez Brunius P, Turrent Thompson C, García Carrillo P. *Escenarios oceánicos y atmosféricos de un derrame de petróleo en aguas profundas del Golfo de México* (Zenodo) (2021). doi:10.5281/zenodo.5745572.
- [18] Norris J. *Markov Chains* (Cambridge University Press) (1998).
- [19] Kovács Z, Tél T. Scaling in multifractals: Discretization of an eigenvalue problem. *Phys. Rev. A* **40** (1989) 4641–4646.
- [20] Koltai P. *Efficient approximation methods for the global long-term behavior of dynamical systems – Theory, algorithms and examples*. Ph.D. thesis, Technical University of Munich (2010).
- [21] Miron P, Beron-Vera FJ, Olascoaga MJ, Koltai P. Markov-chain-inspired search for MH370. *Chaos: An Interdisciplinary Journal of Nonlinear Science* **29** (2019) 041105.
- [22] Helfmann L, Borrell ER, Schütte C, Koltai P. Extending transition path theory: Periodically driven and finite-time dynamics. *J. Nonlinear Sci.* **30** (2020) 3321–3366.
- [23] Abascal AJ, Castanedo S, Medina R, Losada IJ, Alvarez-Fanjul E. Application of HF radar currents to oil spill modelling. *Marine Pollution Bulletin* **58** (2009) 238–248.
- [24] Abascal AJ, Castanedo S, Fernández V, Medina R. Backtracking drifting objects using surface currents from high-frequency (HF) radar technology. *Ocean Dynamics* **62** (2012) 1073–1089.
- [25] Spaulding ML. State of the art review and future directions in oil spill modeling. *Marine Pollution Bulletin* **115** (2017) 7–19.
- [26] ASCE. State-of-the-art review of modeling transport and fate of oil spills. *J. Hydraulic Engr.* **122** (1996) 594–609.
- [27] [Dataset] Offshore Technology. Trion field, Gulf of Mexico. <https://www.offshore-technology.com/projects/trion-oil-field-gulf-of-mexico/> (2020).
- [28] Jouanno J, Ochoa J, Pallas-Sanz E, Sheinbaum J, Andrade-Canto F, Candela J, et al. Loop current frontal eddies: Formation along the Campeche Bank and impact of coastally trapped waves. *J. Phys. Oceanogr.* **46** (2016) 3339–3363.



- [29] [Dataset] Madec G, the NEMO team. NEMO ocean engine. Note du Pole de modelisation de l'Institut Pierre-Simon Laplace, 27, 386 pp., [https://www.nemo-ocean.eu/wp-content/uploads/NEMO\\_book.pdf](https://www.nemo-ocean.eu/wp-content/uploads/NEMO_book.pdf) (2016).
- [30] Gough MK, Beron-Vera FJ, Olascoaga MJ, Sheinbaum J, Juoanno J, Duran R. Persistent transport pathways in the northwestern Gulf of Mexico. *J. Phys. Oceanogr.* **49** (2019) 353–367.
- [31] Duran R, Beron-Vera FJ, Olascoaga MJ. Extracting quasi-steady Lagrangian transport patterns from the ocean circulation: An application to the Gulf of Mexico. *Scientific Reports* **8** (2018) 5218.
- [32] Miron P, Beron-Vera FJ, Olascoaga MJ, Sheinbaum J, Pérez-Brunius P, Froyland G. Lagrangian dynamical geography of the Gulf of Mexico. *Scientific Reports* **7** (2017) 7021.
- [33] Dee DP, Uppala SM, Simmons AJ, Berrisford P, Poli P, Kobayashi S, et al. The ERA-Interim reanalysis: configuration and performance of the data assimilation system. *Quart. J. Roy. Met. Soc.* **137** (2011) 553–597.
- [34] LaCasce JH. Statistics from Lagrangian observations. *Progr. Oceanogr.* **77** (2008) 1–29.
- [35] Tarjan R. Depth-first search and linear graph algorithms. *SIAM J. Comput.* **1** (1972) 146–160.
- [36] Miron P, Beron-Vera FJ, Olascoaga MJ, Froyland G, Pérez-Brunius P, Sheinbaum J. Lagrangian geography of the deep Gulf of Mexico. *J. Phys. Oceanogr.* **49** (2019) 269–290.
- [37] Beron-Vera FJ, Bodnariuk N, Saraceno M, Olascoaga MJ, Simionato C. Stability of the Malvinas Current. *Chaos* **30** (2020) 013152.
- [38] Gómez Ramírez M, Reséndiz Espinosa IN. Seguimiento de nortes en el litoral del Golfo de México en la temporada 1999–2000. *Revista Geográfica* **131** (2002) 5–19.
- [39] Chassignet EP, Hurlburt HE, Smedstad OM, Halliwell GR, Hogan PJ, Wallcraft AJ, et al. The HYCOM (HYbrid Coordinate Ocean Model) data assimilative system. *J. Mar. Sys.* **65** (2007) 60–83.
- [40] [Dataset] National Centers for Environmental Prediction, National Weather Service, NOAA, US Department of Commerce. NCEP GFS 0.25 Degree Global Forecast Grids Historical Archive (2015). doi:10.5065/D65D8PWK.
- [41] Crone TJ, Tolstoy M. Magnitude of the 2010 Gulf of Mexico oil leak. *Science* **330** (2010) 634. doi:10.1126/science.1195840.
- [42] Streett D. NOAA's Satellite Monitoring of Marine Oil. *Geophysical Monograph Series* **195** (2011) 9–18.
- [43] [Dataset] Ko DS, Preller RH, Martin PJ. An experimental real-time Intra-Americas Sea Ocean Nowcast/Forecast System for coastal prediction. *Proceedings of the AMS 5th Conference on Coastal Atmospheric and Oceanic Prediction and Processes*, pp. 97–100. (2003).
- [44] Zhang HM, Bates JJ, Reynolds RW. Assessment of composite global sampling: Sea surface wind speed. *Geophysical Research Letters* **33** (2006) L17714.
- [45] Lumpkin R, Pazos M. Measuring surface currents with Surface Velocity Program drifters: the instrument, its data and some recent results. Griffa A, Kirwan AD, Mariano A, Özgökmen T, Rossby T, editors, *Lagrangian Analysis and Prediction of Coastal and Ocean Dynamics* (Cambridge University Press), chap. 2 (2007), 39–67.
- [46] Lumpkin R, Grodsky SA, Centurioni L, Rio MH, Carton JA, Lee D. Removing spurious low-frequency variability in drifter velocities. *J. Atm. Oce. Tech.* **30** (2012) 353–360.
- [47] Olascoaga MJ, Beron-Vera FJ, Haller G, Trinanes J, Iskandarani M, Coelho EF, et al. Drifter motion in the Gulf of Mexico constrained by altimetric Lagrangian Coherent Structures. *Geophys. Res. Lett.* **40** (2013) 6171–6175.

- [48] Graber HC, Haus BK, Chapman RD, Shay LK. Hf radar comparisons with moored estimates of current speed and direction: Expected differences and implications. *Journal of Geophysical Research: Oceans* **102** (1997) 18749–18766.
- [49] Röhrs J, Sperrevik AK, Christensen KH, Broström G, Breivik O. Comparison of HF radar measurements with Eulerian and Lagrangian surface currents. *Ocean Dyn.* **65** (2015) 679–690.
- [50] Beron-Vera FJ, Olascoaga MJ, Miron P. Building a Maxey–Riley framework for surface ocean inertial particle dynamics. *Phys. Fluids* **31** (2019) 096602.
- [51] Olascoaga MJ, Beron-Vera FJ, Miron P, Triñanes J, Putman NF, Lumpkin R, et al. Observation and quantification of inertial effects on the drift of floating objects at the ocean surface. *Phys. Fluids* **32** (2020) 026601.
- [52] Dagestad KF, Rohrs J, Breivik O, Adlandsvik B. OpenDrift v1.0: a generic framework for trajectory modelling. *Geoscientific Model Development* **11** (2018) 1405–1420.
- [53] Romo-Curiel A, Ramirez-Mendoza Z, Fajardo-Yamamoto A, Ramirez-Leon M, García-Aguilar M, Herzka S, et al. Assessing the exposure risk of large pelagic fish to oil spills scenarios in the deep waters of the gulf of mexico. *Marine Pollution Bulletin* **176** (2022) 113434.